International Journal of Engineering Science 99 (2016) 74–91

Contents lists available at ScienceDirect

International Journal of Engineering Science

journal homepage: www.elsevier.com/locate/ijengsci

Modeling and efficient simulation of the deposition of particulate flows onto compliant substrates

T.I. Zohdi*

Department of Mechanical Engineering, University of California, Berkeley, CA 94720-1740, USA

ARTICLE INFO

Article history:
Received 17 October 2015
Accepted 19 October 2015

Keywords:
particles
substrates
computation
deposition
manufacturing

ABSTRACT

There are many emerging manufacturing processes whereby structures are formed by depositing materials onto substrates in order to build up layers or coatings. The processes are often referred to as "additive manufacturing". Particle-based additive manufacturing processes utilize deposition of streams of particles to build layers upon substrate surfaces. Oftentimes, the substrates are fragile/sensitive, and could become damaged if the induced stresses due to deposition are too high. In these cases, knowledge of the substrate stresses is important. This paper develops a computational-mechanics framework to *rapidly* evaluate the induced substrate stresses due to multiple, simultaneous, surface particle contact events. The aggregate substrate stresses are efficiently computed by superposing individual particle contact solutions, based on classical Boussinesq solutions, coupled to a multibody dynamics formulation for the interacting particles. The utility of the approach is that process designers can efficiently compute the results of selecting various system parameters, such as deposition speed, particle-stream configuration, etc. This allows one to rapidly compute system parameter studies needed in new product development. Three-dimensional examples are provided to illustrate the technique.

1. Introduction

There are a variety of advanced multi-step manufacturing processes which utilize deposition particles onto a surface in order to build a component. These are known as "additive" (adding material) manufacturing methods.[1] In 2014, print-based additive manufacturing technologies, which often employ deposition of particulate materials, such as ceramics, metals, plastics, organics and biological materials was a 2.2 billion dollar industry. In certain applications, because the substrate is fragile, knowledge of the induced stresses is important in order to control the process (Fig. 1). Such concerns have become increasingly important due to the rise of printed flexible electronics involving sensitive, potentially fragile dielectric and optical materials. Applications include, for example, optical coatings and photonics (Nakanishi et al., 2009), MEMS applications (Fuller, Wilhelm, & Jacobson, 2002) and (Samarasinghe, Pastoriza-Santos, Edirisinghe, Reece, & Liz-Marzan, 2006) and even biomedical devices (Ahmad, Rasekh, & Edirisinghe, 2010). There are a wide variety of additive-like processes and we refer the reader to Gamota, Brazis, Kalyanasundaram, and Zhang (2004), Sirringhaus et al. (2000), Wang, Zheng, Li, Huck, and Sirringhaus (2004), Huang, Liao, Molesa, Redinger, and Subramanian (2003), Choi et al. (2010a), Choi, Stassi, Pisano, and Zohdi (2010b), Choi et al. (2012),

* Tel.: +15106429172.
E-mail address: zohdi@berkeley.edu

[1] This is opposite to classical "subtractive" processes whereby material is removed (such as milling) to build a component.

http://dx.doi.org/10.1016/j.ijengsci.2015.10.012
0020-7225/

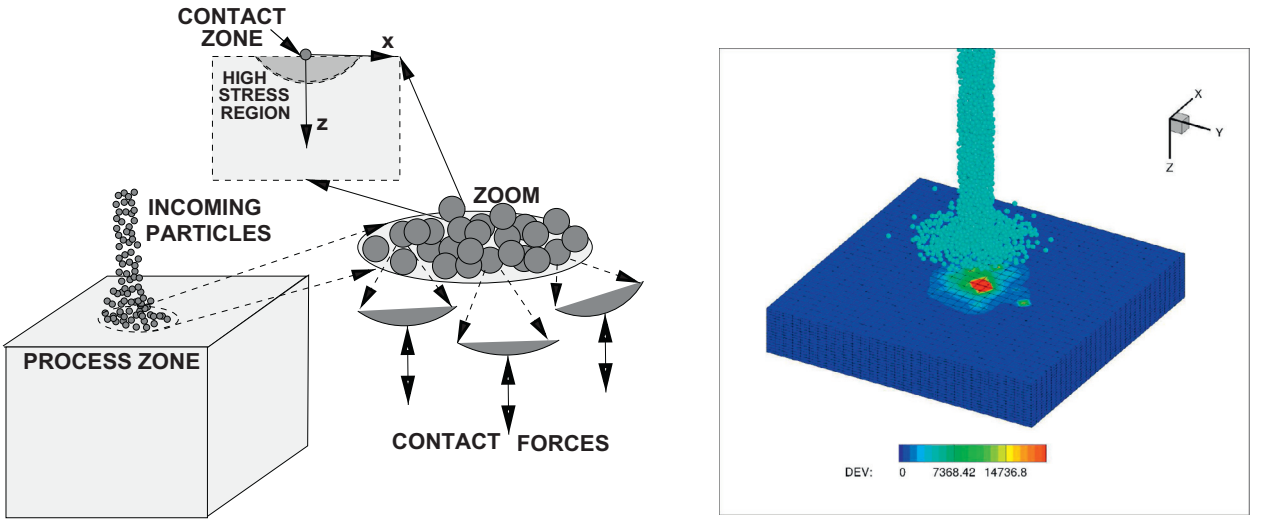

Fig. 1. LEFT:Deposition of a stream of particles onto a substrate. RIGHT: An example of a set of particles inducing loads through surface contact from a deposition of a stream from the simulations presented later.

Choi, Pisano, and I. (2013), Demko, Choi, Zohdi, and Pisano (2012), Demko, Cheng, and Pisano (2010), Fathi, Dickens, Khodabakhshi, and Gilbert (2013), Martin (2009), Martin (2011) and Zohdi (2014d), Zohdi (2014b), Zohdi (2015a) for details. These types are similar to those in the area spray coatings. We refer the reader to the extensive works of Sevostianov and Kachanov (2000), Sevostianov and Kachanov (2001b), Sevostianov and Kachanov (2001a), Nakamura and coworkers: Dwivedi, Wentz, Sampath, and Nakamura (2010), Liu, Nakamura, Dwivedi, Valarezo, and Sampath (2008), Liu et al. (2007), Nakamura and Liu (2007), Nakamura, Qian, and Berndt (2000) and Qian, Nakamura, and Berndt (1998) and to Martin (2009), Martin (2011) for the state of the art in deposition technologies. Oftentimes, the objective is to produce multilayer coatings on curved surfaces (see, for example Grekov & Kostyrko, 2015). The interested reader is referred to the recent overview article by Huang, Leu, Mazumdar, and Donmez (2015) on the wide array of activities in additive manufacturing. This paper develops a computational-mechanics framework to investigate the behavior of such processes. Specifically, substrate stresses due to multiple, simultaneous, surface particle contact events are efficiently computed by superposing individual particle contact solutions, based on classical Boussinesq-like solutions, coupled to a multibody dynamics formulation for the interacting particles. Specifically, in the paper:

- A multibody collision model is used to represent the interaction of the particles with each other, as well as with the substrate.
- Classical point-load solutions on a half-space are used to represent the contribution of each particle to the stresses on the substrate.
- The response of the particles and substrate are coupled together with a recursive numerical scheme.
- Three-dimensional examples are provided to illustrate the technique.

Remark. The modeling approach allows for rapid computation of deposition-induced stresses which allows one to conduct parameter studies, leaving more intensive Finite Element analyses, if warranted, for final process analysis stages. We note that the range of validity of this type of simulation is for relatively slow deposition where elastodynamic effects can be ignored in the substrate. Furthermore, we consider "dry" particle depositions where the interstitial fluid is of negligible importance. Particles in suspension are outside the scope of this paper. We refer the reader to Kachanov and Abedian (2015), Abedian and Kachanov (2010) and Sevostianov and Kachanov (2012) for details on the analysis of that class of particle-laden fluid materials. Such analyses can be useful for determining the rheology of so-called (particle) functionalized-inks (Zohdi, 2014a).

2. A multibody dynamics model for the particles

2.1. Overall contributing forces

We consider a group of non-intersecting particles ($i = 1, 2, \ldots, N_p$). The objects in the system are assumed to be small enough to be considered (idealized) as particles, spherical in shape, and that the effects of their rotation with respect to their mass center is unimportant to their overall motion, although, we will make further remarks on these effects shortly. The equation of motion for the i^{th} particle in system is

$$m_i \ddot{\mathbf{r}}_i = \boldsymbol{\Psi}_i^{tot}(\mathbf{r}_1, \mathbf{r}_2, \ldots, \mathbf{r}_{N_p}) = \boldsymbol{\Psi}_i^{con} + \boldsymbol{\Psi}_i^{subs} + \boldsymbol{\Psi}_i^{bond} + \boldsymbol{\Psi}_i^{damp}, \tag{1}$$

where $\mathbf{r}_i$ is the position vector of the i^{th} particle and where $\boldsymbol{\Psi}_i^{tot}$ represents all forces acting on particle i, which is decomposed into the sum of forces due to:

- Inter-particle forces (Ψ_i^{con}) generated by contact with other particles,
- Substrate forces (Ψ_i^{subs}) generated by contact with constraining surfaces,
- Adhesive bonding forces (Ψ_i^{bond}) with other particles and the substrate,
- Damping forces arising from the surrounding interstitial environment (Ψ_i^{damp}) occurring from potentially viscous, surrounding, interstitial fluids and surfactants.

Following the approach in Zohdi (2014b, 2014c), in the next sections, we examine of each of the types of forces in the particle system in detail.

Remark. For the interested reader, we remark that there are a variety other particle-based modeling methods, usually referred to as Discrete Element Methods. For example see Avci and Wriggers (2012); Bolintineanu et al. (2014); Cante et al. (2014); Carbonell, Onate, and Suarez (2010); Labra and Onate (2009); Leonardi, Wittel, Mendoza, and Herrmann (2014); Onate, Celigueta, Idelsohn, Salazar, and Suárez (2011); Onate et al. (2014); Onate, Idelsohn, Celigueta, and Rossi (2008); Rojek (2014); Rojek, Labra, Su, and Onate (2012) and Zohdi (2002, 2005, 2007, 2015a).

2.2. Comments on rotations

The introduction of rolling and spin is questionable for a small object, idealized by a particle, in particular because of rolling resistance. In addition to the balance of linear momentum, $m_i\dot{\mathbf{v}}_i = \Psi_i^{tot}$, where the $\mathbf{v}_i$ is the velocity of the center of mass, the equations of angular momentum read $\dot{\boldsymbol{H}}_{i,cm} = \frac{d(\bar{I}_i\cdot\boldsymbol{\omega}_i)}{dt} = \boldsymbol{M}_{i,cm}^{tot}$. For spheres, we have $\boldsymbol{H}_{i,cm} = \bar{I}_{i,s}\boldsymbol{\omega}_i = \frac{2}{5}m_iR_i^2\boldsymbol{\omega}_i$ and for the time discretization

$$\boldsymbol{\omega}_i(t+\Delta t) = \boldsymbol{\omega}_i(t) + \frac{\Delta t}{\bar{I}_{i,s}}\Big(\phi\boldsymbol{M}_{i,cm}^{tot}(t+\Delta t) + (1-\phi)\boldsymbol{M}_{i,cm}^{tot}(t)\Big), \tag{2}$$

where $\boldsymbol{M}_{i,cm}^{tot}$ are the total moments generated by interaction forces, such as contact forces, rolling resistance, etc. For the applications at hand, the effects of rolling is generally negligible, in particular because the particles are small. However, nonetheless, we formulate the system with rotations where $\mathbf{r}_i$ is the position of the center of mass, $\mathbf{v}_i$ is the velocity of the center of mass and $\boldsymbol{\omega}_i$ is the angular velocity. An important quantity of interest is the velocity on the surface of the "particles", which is a potential contact point with other particles, denoted $\boldsymbol{v}_i^c$

$$\boldsymbol{v}_i^c = \boldsymbol{v}_i + \boldsymbol{\omega}_i \times \mathbf{r}_{i\rightarrow c}, \tag{3}$$

where $\mathbf{r}_{i\rightarrow c}$ is the relative position vector from the center to the possible point of contact. This is discussed further later.

2.3. Particle-to-particle contact forces

Following (Zohdi, 2014b, 2014c), we employ a simple particle overlap model to determine the normal contact force contributions from the surrounding particles (N_{ci}) in contact, $\Psi_i^{con,n} = \sum_{j=1}^{N_{ci}} \boldsymbol{\psi}_{ij}^{con,n}$, based on separation distance between particles in contact (Fig. 2). Generally,

$$\boldsymbol{\Psi}_{ij}^{con,n} = \mathcal{F}(||\mathbf{r}_i - \mathbf{r}_j||, R_i, R_j, \text{material parameters}). \tag{4}$$

There is no shortage of contact models, of varying complexity, to generate a contact interaction force. Throughout this work, we will utilize a particularly simple relation whereby contact force is proportional to the relative *normalized* proximity of particles i and j in contact, detected by the distance between centers being less than the sum of the radii

$$\text{If } ||\mathbf{r}_i - \mathbf{r}_j|| \leq R_i + R_j \Rightarrow \text{activate contact}, \tag{5}$$

where we define the overlap as

$$\delta_{ij} \stackrel{\text{def}}{=} |||\mathbf{r}_i - \mathbf{r}_j|| - (R_i + R_j)|. \tag{6}$$

Accordingly, we consider the following

$$\boldsymbol{\Psi}_{ij}^{con,c} \propto -K_{pij}|\mathcal{E}_{ij}|^{p_p}\mathbf{n}_{ij}A_{ij}^c, \tag{7}$$

where $0 < K_{pij} < \infty$ is a particle-to-particle contact compliance constant, p_p is a material parameter, $\mathcal{E}_{ij}$ is normalized/nondimensional (strain-like) deformation metric

$$\mathcal{E}_{ij} = |\frac{||\mathbf{r}_i - \mathbf{r}_j|| - (R_i + R_j)}{(R_i + R_j)}| = \frac{\delta_{ij}}{(R_i + R_j)} \tag{8}$$

and

$$\mathbf{n}_{ij} = -\frac{\mathbf{r}_i - \mathbf{r}_j}{||\mathbf{r}_i - \mathbf{r}_j||} = \frac{\mathbf{r}_j - \mathbf{r}_i}{||\mathbf{r}_i - \mathbf{r}_j||}, \tag{9}$$

where the R_i and R_j are the radii of particles i and j respectively. The term A_{ij}^c is a contact area parameter, which is discussed in Appendix B. Appendix B also provides a brief review of alternative models, such as the classical Hertzian contact model.

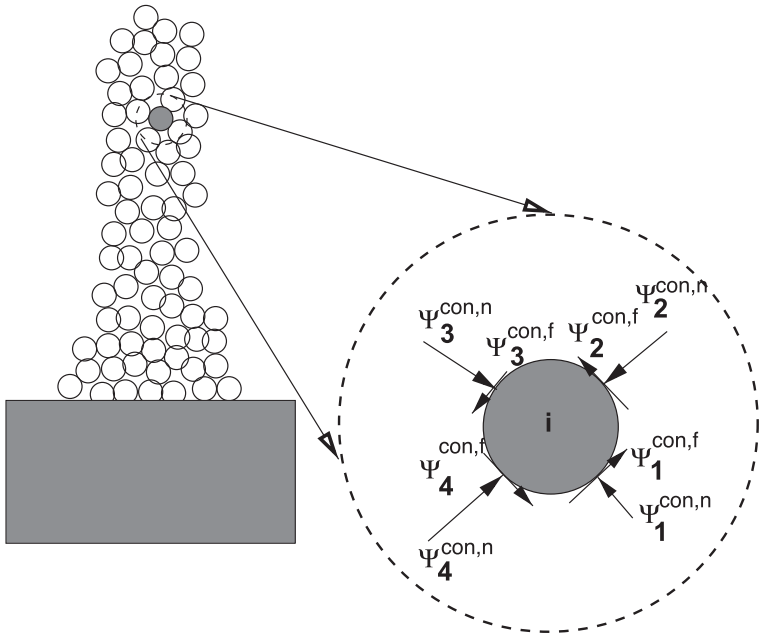

Fig. 2. Normal contact and friction forces induced by neighboring particles in contact (after Zohdi, 2014b, 2014c).

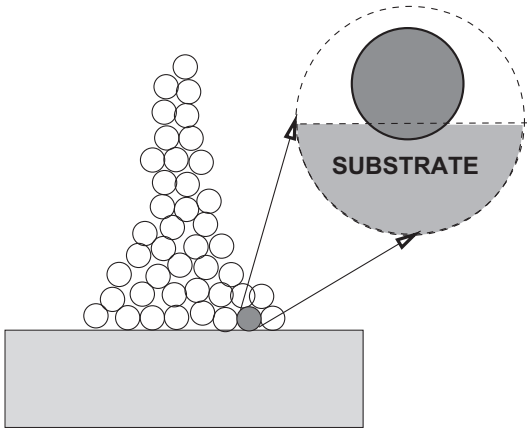

Fig. 3. An example of overlap model for contact force determination between a substrate and a particle. The amount of overlap of the particle with the substrate position dictating the force (Zohdi, 2014b, 2014c).

2.3.1. Particle-substrate contact

Contact of a particle-to-substrate contact is handled in the identical manner to particle-to-particle, except that the substrate displacement is considered given (externally controlled), and independent of the action with the particles. The contact between the substrate and the particles is handled exactly in the same manner as the particle to particle contact, with the amount of overlap of the particle with the substrate position dictating the force (see Fig. 3).

2.3.2. Contact dissipation

Phenomenological particle contact dissipation can be incorporated by tracking the relative velocity of the particles in contact. A simple model to account for this is

$$\boldsymbol{\Psi}_{ij}^{con,d} = c^{cd}(\boldsymbol{v}_{nj} - \boldsymbol{v}_{ni})A_{ij}^{c} \tag{10}$$

2.4. Regularized contact friction models

Frictional stick is modeled via the following regularized friction algorithm: (at the point of contact)

- Check static friction threshold (K^f is a tangential contact friction compliance constant):

$$K^f||\boldsymbol{v}^c_{j,\tau} - \boldsymbol{v}^c_{i,\tau}||A^c_{ij}\Delta t \text{ against } \mu_s||\boldsymbol{\Psi}^{con,n}||, \tag{11}$$

where $||\boldsymbol{v}^c_{j,\tau} - \boldsymbol{v}^c_{i,\tau}||\Delta t$ (of dimensions of length) is the relative tangential velocity at a point of contact, Δt is the time-step used later in the numerical discretization, μ_s is the static friction coefficient. *This step replaces ("regularizes") a more rigorous, and difficult, step of first assuming no slip, generating the no-slip contact forces, by solving an entire multibody/multisurface contact problem, $\boldsymbol{\Psi}^{ns}$, and checking Ψ^{ns} against the threshold $\mu_s||\boldsymbol{\Psi}^{con,n}||$ on each surface.*

- If the threshold is not met ($K^f||\boldsymbol{v}^c_{j,\tau} - \boldsymbol{v}^c_{i,\tau}||A^c_{ij}\Delta t < \mu_s||\boldsymbol{\Psi}^{con,n}||$), then

$$\boldsymbol{\Psi}^{con,f} = K^f||\boldsymbol{v}^c_{j,\tau} - \boldsymbol{v}^c_{i,\tau}||A^c_{ij}\Delta t\boldsymbol{\tau}^c_{ij} \tag{12}$$

where

$$\boldsymbol{\tau}^c_{ij} = -\frac{\boldsymbol{v}^c_{i,\tau} - \boldsymbol{v}^c_{j,\tau}}{||\boldsymbol{v}^c_{j,\tau} - \boldsymbol{v}^c_{i,\tau}||} = \frac{\boldsymbol{v}^c_{j,\tau} - \boldsymbol{v}^c_{i,\tau}}{||\boldsymbol{v}^c_{j,\tau} - \boldsymbol{v}^c_{i,\tau}||}, \tag{13}$$

where the subscripts indicate the tangential components of velocity. The tangential velocity at the contact point is obtained by subtracting away the normal component of the velocity

$$\boldsymbol{v}^c_t = \boldsymbol{v}^c - (\boldsymbol{v}^c \cdot \boldsymbol{n})\boldsymbol{n}. \tag{14}$$

- If the threshold is met or exceeded ($K^f||\boldsymbol{v}^c_{j,\tau} - \boldsymbol{v}^c_{i,\tau}||A^c_{ij}\Delta t \geq \mu_s||\boldsymbol{\Psi}^{con,n}||$), then one adopts a slip model of the form

$$\boldsymbol{\Psi}^{con,f}_{ij} = \mu_d||\boldsymbol{\Psi}^{con,n}_{ij}||\boldsymbol{\tau}^c_{ij}, \tag{15}$$

where μ_d is the dynamic friction coefficient.

2.5. Particle-to-particle bonding relation

In some cases, we may wish to consider particles to bond to one another, and we adopt a criterion based on exceeding a critical interpenetration distance. Explicitly:

- Recall, if $||\boldsymbol{r}_i - \boldsymbol{r}_j|| \leq (R_i + R_j)$, then the particles are in contact and $\mathcal{E}_{ij} = \frac{\delta_{ij}}{(R_i+R_j)}$.
- If the particles are in contact and $|\mathcal{E}_{ij}| \geq \mathcal{E}^*$, then an (adhesive/attractive) normal bond is activated between the particles of the form

$$\boldsymbol{\Psi}^{bond,n}_{ij} = K^{nb}_{ij}|\mathcal{E}_{ij}|^{p_b}\boldsymbol{n}_{ij}A^c_{ij}, \tag{16}$$

where $0 \leq K^{nb}_{ij}$ is a bonding constant and p_b is a material parameter.

- If the particles have an activated normal bond, then the particles automatically have a rotational bond equivalent in form to stick friction

$$\boldsymbol{\Psi}^{bond,r}_{ij} = K^{rb}_{ij}||\boldsymbol{v}^c_{j,\tau} - \boldsymbol{v}^c_{i,\tau}||A^c_{ij}\Delta t\boldsymbol{\tau}^c_{ij}. \tag{17}$$

Remark. Of course such a bond model can immediately be used for a particle and a substrate surface.

2.6. Interstitial damping

Finally, we note that damping from interstitial fluid (or even smaller-scale paricles, solvents) between particles, such as binding enhancers, surfactants and lubricants is possible. A simple model to account for this is (a Stokesian, low Reynolds number, model)

$$\boldsymbol{\Psi}^{damp}_i = c^e 6\pi R_i(\boldsymbol{v}^e - \boldsymbol{v}_i) \tag{18}$$

where $\mathbf{v}^e$ is the local average velocity of the external interstitial medium, which one may assume to be $\mathbf{v}^e \approx \mathbf{0}$, for most applications of interest.[2] The mechanics of the interstitial fluid is unimportant in the current analysis. Clearly, for other applications, such as high-speed flow, the motion of the fluid can be important, requiring more sophisticated drag laws and/or fully coupled (two-way) particle-fluid interaction models. This is outside the scope of the present work. Generally, this requires the use of solid-fluid staggering-type schemes (for example, see Zohdi, 2014a, 2007 and Avci and Wriggers, 2012).

3. Induced substrate stresses

Our basic approach is to represent the contribution of the contact induced by each particle as a point-load on an infinite half space. We break the point load into two components: (1) the normal load and the (2) tangential load. Afterwards, we sum all of the contributions to obtain the total induced stress field in the substrate.

[2] c^e is usually the viscosity of the fluid.

3.1. Individual particle contributions-normal load

The corresponding radially-symmetric (θ-independent) solution (Fig. 1) for a normal load at $(x, y, z) = (0, 0, 0)$ in the z-direction is (in cylindrical coordinates, Boussinesq, 1885)[3]:

$$
\begin{aligned}
\sigma_{rr} &= \frac{F_z}{2\pi}\left((1-2\nu)\left(\frac{1}{r^2}-\frac{z}{\gamma r^2}\right)-\frac{3zr^2}{\gamma^5}\right),\\
\sigma_{\theta\theta} &= -\frac{F_z}{2\pi}(1-2\nu)\left(\frac{1}{r^2}-\frac{z}{\gamma r^2}-\frac{z}{\gamma^3}\right),\\
\sigma_{zz} &= -\frac{3F_z}{2\pi}\frac{z^3}{\gamma^5},\\
\sigma_{rz} &= -\frac{3F_z}{2\pi}\frac{rz^2}{\gamma^5},\\
\sigma_{r\theta} &= 0 \quad \text{(symmetry)},\\
\sigma_{z\theta} &= 0 \quad \text{(symmetry)},
\end{aligned}
\tag{19}
$$

where $r \stackrel{\text{def}}{=} \sqrt{x^2+y^2}$ and $\gamma \stackrel{\text{def}}{=} \sqrt{x^2+y^2+z^2}$.

Remark. Often it is convenient to move back and forth from Cartesian and Cylindrical bases, which can be achieved by simply rotating the system with

$$
\boldsymbol{\sigma}^{cart}(\theta) = \boldsymbol{R}^T(\theta)\cdot\boldsymbol{\sigma}^{cyl}\cdot\boldsymbol{R}(\theta),
\tag{20}
$$

where $\mathbf{R}(\theta)$ is defined as

$$
\boldsymbol{R}(\theta) \stackrel{\text{def}}{=} \begin{bmatrix} cos\theta & sin\theta & 0\\ -sin\theta & cos\theta & 0\\ 0 & 0 & 1\end{bmatrix},
\tag{21}
$$

and where $\boldsymbol{R}^T(\theta) = \boldsymbol{R}^{-1}(\theta)$, because it is an orthonormal matrix[4].

3.2. Individual particle contributions-tangential load

The effects of non-normal (tangential) loadings can be included by utilizing the solutions for a tangential point load in the $x-$direction (see Kachanov et al., 2003 for reviews):

$$
\begin{aligned}
\sigma_{xx} &= \frac{F_x}{2\pi}\left(-3\frac{x^3}{\gamma^5}+(1-2\nu)\left(\frac{x}{\gamma^3}-\frac{3x}{\gamma(\gamma+z)^2}+\frac{x^3}{\gamma^3(\gamma+z)^2}+\frac{2x^3}{\gamma^2(\gamma+z)^3}\right)\right)\\
\sigma_{yy} &= \frac{F_x}{2\pi}\left(-3\frac{xy^2}{\gamma^5}+(1-2\nu)\left(\frac{x}{\gamma^3}-\frac{x}{\gamma(\gamma+z)^2}+\frac{xy^2}{\gamma^3(\gamma+z)^2}+\frac{2xy^2}{\gamma^2(\gamma+z)^3}\right)\right)\\
\sigma_{zz} &= -\frac{3F_x}{2\pi}\frac{xz^2}{\gamma^5}\\
\sigma_{xy} &= \frac{F_x}{2\pi}\left(-3\frac{x^2y}{\gamma^5}+(1-2\nu)\left(-\frac{y}{\gamma(\gamma+z)^2}+\frac{x^2y}{\gamma^3(\gamma+z)^2}+\frac{2x^2y}{\gamma^2(\gamma+z)^3}\right)\right)\\
\sigma_{yz} &= -\frac{3F_x}{2\pi}\frac{xyz}{\gamma^5}\\
\sigma_{zx} &= -\frac{3F_x}{2\pi}\frac{x^2z}{\gamma^5}
\end{aligned}
\tag{22}
$$

and performing a coordinate transformation (to a tilde-frame) $\tilde{x} = y$, $\tilde{y} = x$,$\tilde{z} = z$ to account for any F_y loading in the $y-$direction. The results from the loading in the x, y and z directions can be superposed to produce the total loading.

[3] See (Kachanov, Shafiro, & Tsukrov, 2003) for a complete, rigorous, derivation.

[4] We note that the quantity $\boldsymbol{\sigma}'$: $\boldsymbol{\sigma}'$ is invariant under the rotational coordinate transformation, in other words, $\boldsymbol{\sigma}'^{,car}$: $\boldsymbol{\sigma}'^{,car} = (\boldsymbol{R}^T(\theta)\cdot\boldsymbol{\sigma}'^{,cyl}\cdot\boldsymbol{R}(\theta))^T$: $(\boldsymbol{R}^T(\theta)\cdot\boldsymbol{\sigma}'^{,cyl}\cdot\boldsymbol{R}(\theta)) = \boldsymbol{\sigma}'^{,cyl}$: $\boldsymbol{\sigma}'^{,cyl}$, thus this metric remains perfectly acceptable to use in the presence of non-normal loading.

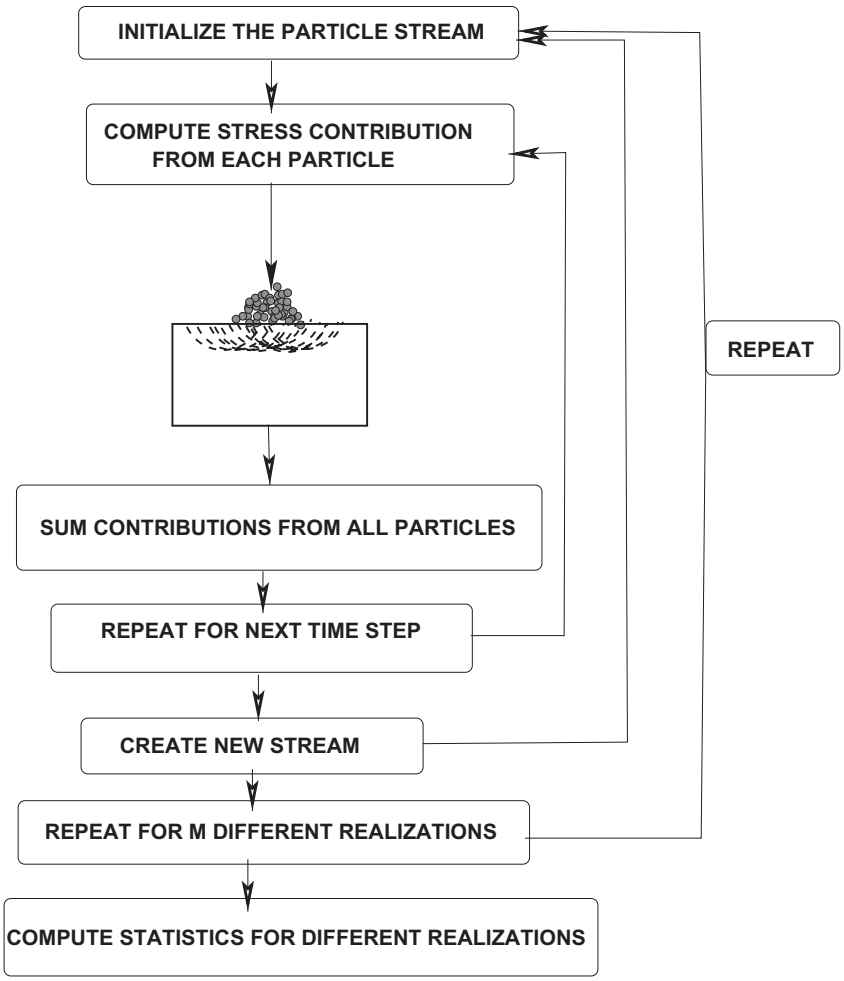

Fig. 4. The algorithm for computation of the loading of a surface.

3.3. Superposition of contributions for the total substrate stresses

The total stress at a point in the substrate is computed by summing all point load (particle) contributions ($I = 1, 2, \ldots, N$, appropriately translated according to their position on the surface):

$$\boldsymbol{\sigma}_{tot\text{-}N}(\boldsymbol{x}) = \sum_{I=1}^{N} \boldsymbol{\sigma}_I(\boldsymbol{x}), \tag{23}$$

where the contact forces will be determined from the soultion of the multibody particle problem (Appendix A). We assume that there is only normal loading. The presence of tangential loading is discussed in the conclusions. From Eq. (19) one can determine the von Mises stress $(\boldsymbol{\sigma}_{tot-N})' = \sum_{I=1}^{N} \boldsymbol{\sigma}_I'$, where $\boldsymbol{\sigma}_I' = \boldsymbol{\sigma}_I - \frac{tr\boldsymbol{\sigma}_I}{3}\mathbf{1}$, which is usually important for failure assessment.

The computational algorithm is as follows:

- INITIALIZATION: GENERATE A STARTING CONFIGURATION FOR THE PARTICLES
- STEP 1: COMPUTE THE FORCES FROM PARTICLES IN CONTACT WITH THE SURFACE-THIS PRODUCES N LOADING SITES.
- STEP 2: COMPUTE THE STRESS FIELD CONTRIBUTION FROM EACH PARTICLE, $I = 1, 2, \ldots N$, ON THE SURFACE.
- STEP 3: SUM THE CONTRIBUTIONS OF EACH PARTICLE, $I = 1, 2, \ldots N$, TO COMPUTE THE TOTAL.
- STEP 4: REPEAT STEPS 1–3 FOR EACH TIME STEP.
- STEP 5: COMPUTE THE SUBSTRATE RESPONSE STATISTICS IN THE TARGET ZONE OF INTEREST AS DESIRED.

Fig. 4 provides a corresponding flow chart for the process. The utility of the approach is that one can ascertain detailed spatial distribution of the stresses in the substrate. One can also post-process aggregate stresses. For example, one statistical metric is

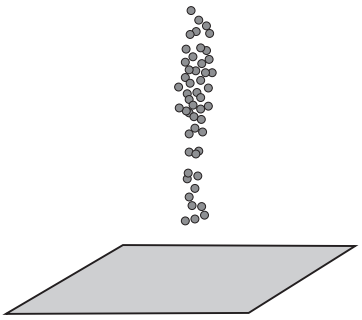

Fig. 5. The deposition scenario.

the volume average deviatoric stress metric in the volume with N surface load particles at any given moment in time:

$$\langle (\boldsymbol{\sigma}_{tot-N})' : (\boldsymbol{\sigma}_{tot-N})' \rangle_{\Omega} \stackrel{\text{def}}{=} \sqrt{\frac{1}{|\Omega|} \int_{\Omega} (\boldsymbol{\sigma}_{tot-N})' : (\boldsymbol{\sigma}_{tot-N})' \, dV}. \tag{24}$$

Remark. In Appendix A, a numerical method based on an iterative solution scheme found in Zohdi (2014a, 2002, 2005, 2007, 2010, 2012, 2013a, 2013b, 2014b, 2014c, 2014d, 2015a, 2015b); Zohdi and Wriggers (2008) is presented to solve for the multibody dynamics of the particles.

4. Numerical examples

We consider a model problem of an initially cylindrical stream of equally-sized particles (Fig. 5) to illustrate the process. The absolute dimensions are unimportant for the model problem, and have been normalized so that the initial droplet diameter was on the order of unity. The relevant simulation parameters chosen were (in SI-units if not explicitly stated, see Appendix A):

- The particle radii, $R_i = 0.05$ m,
- The normal contact parameter was $K_{po} = 10^7 \text{N/m}^2$, at a fixed temperature, $K_p = \mathbf{MAX}(K_{po}(e^{-a\frac{\Theta}{\Theta^*}-1}), K_p^{lim})$, where $\Theta^* = 500^o$ K, $K_p^{lim} = 10^6 \text{N/m}^2$ and the exponent in the contact law was set to $p_p = 2$,
- The stiffness of the wall in contact law, $K_w = 10^9 \text{N/m}^2$,
- The contact damping parameter, $c^{cd} = 10^5$,
- The friction contact parameter $K^f = 10^7$,
- The coefficient of static friction, $\mu_s = 0.4$,
- The coefficient of dynamic friction, $\mu_d = 0.3$,
- The normal bond parameter, $K^{nb} = 10^6 \text{N/m}^2$ and the exponent in the binding law was set to $p_b = 2$,
- The rotational bond parameter, $K^{rb} = 10^3$,
- The interstitial damping coefficient $c^e = 1$ (assumed Stokesian-like),
- The target number of fixed point iterations, $K_d = 10$,
- The trapezoidal time-stepping parameter, $\phi = 0.5$,
- The simulation duration, 2 s,
- The initial time step size, 0.00025 s,
- The time step upper bound, 0.00025 s and
- The tolerance for the fixed-point iteration, 5×10^{-4}.

All system parameters can be scaled to describe any specific system of interest. They were selected simply for illustration purposes. In order to generate an initial particle configuration, we randomly dispersed $N_p = 2000$ non-overlapping particles within a cylindrical domain, then projected them onto the surface. The configuration of the sample, before it was dropped, was generated using a classical Random Sequential Addition (RSA) algorithm (Widom, 1966), which places non-overlapping particles randomly into the domain of interest. One could start with a denser starting configuration by using equilibrium-driven Metropolis algorithm or alternative methods based on simultaneous particle flow and growth (see Donev et al., 2004a; Donev, Stillinger, Chaikin, and Torquato, 2004b; Donev, Torquato, and Stillinger, 2005; Kansaal, Torquato, and Stillinger, 2002 and Torquato, 2002), although this was not necessary for this example. As an example, deposition of a stream of particles (Fig. 5) is dropped onto a lower surface (by gravity with an initial uniform downward velocity), and allowed to freely spread/deform according to its interaction with the surface (Figs. 6, 7, 8). The substrate colors indicate the norm of the total summed deviatoric stresses. Both the top (left) and bottom (right) are shown. The localized nature of the surface stresses are smeared out with increasing depth. All computations were run in a matter of a few minutes on a laptop.

Remarks. A rigorous, detailed analysis of the deformation and stress within an impacted substrate is an extremely complex process, requiring a finite element analysis of the deformation of contacting bodies. We refer the reader to Wriggers (2002) for

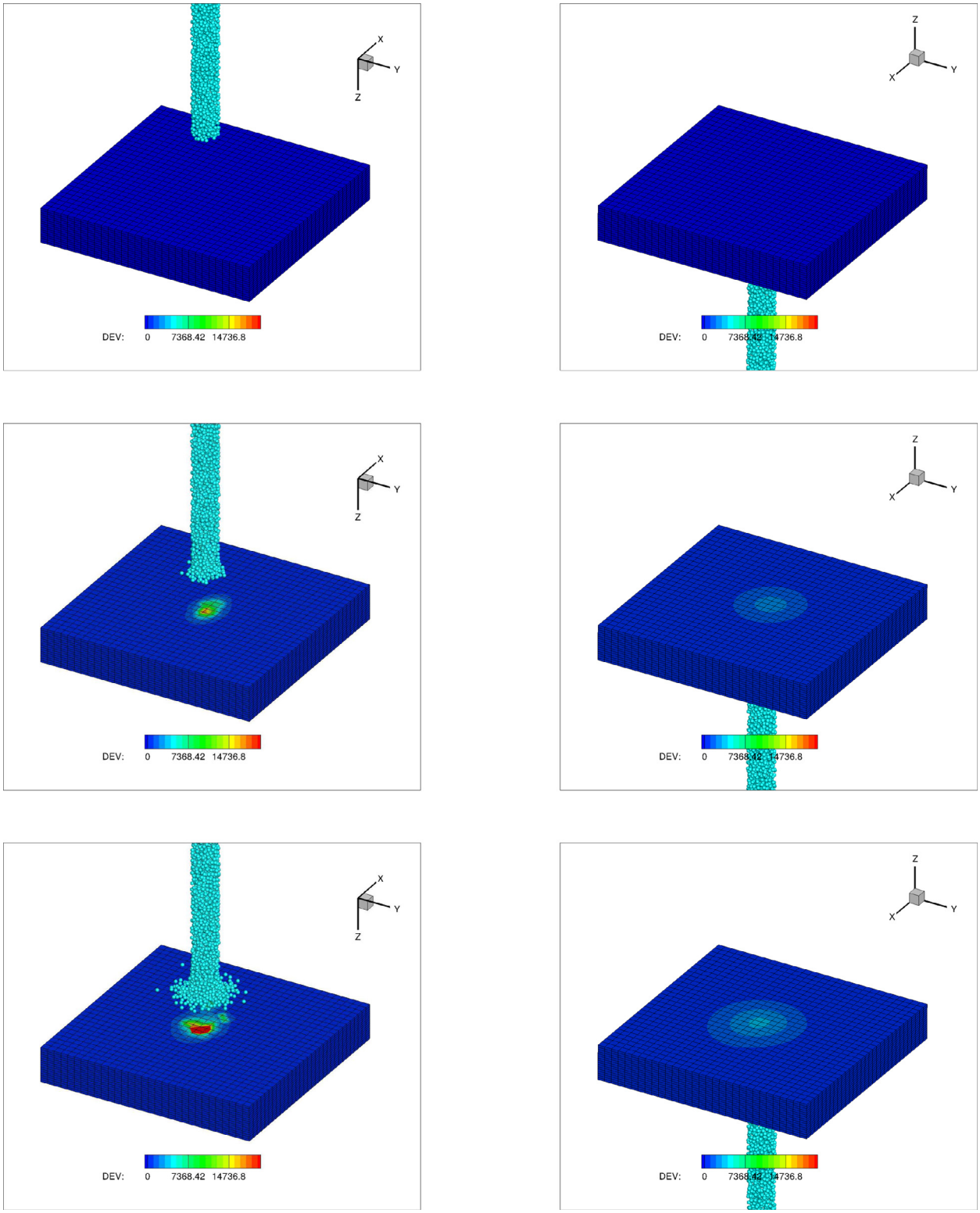

Fig. 6. Example: Deposition onto a surface. . The substrate colors indicate the norm of the total summed deviatoric stresses. Both the top (left) and bottom (right) are shown. The localized nature of the surface stresses are smeared out with increasing depth.

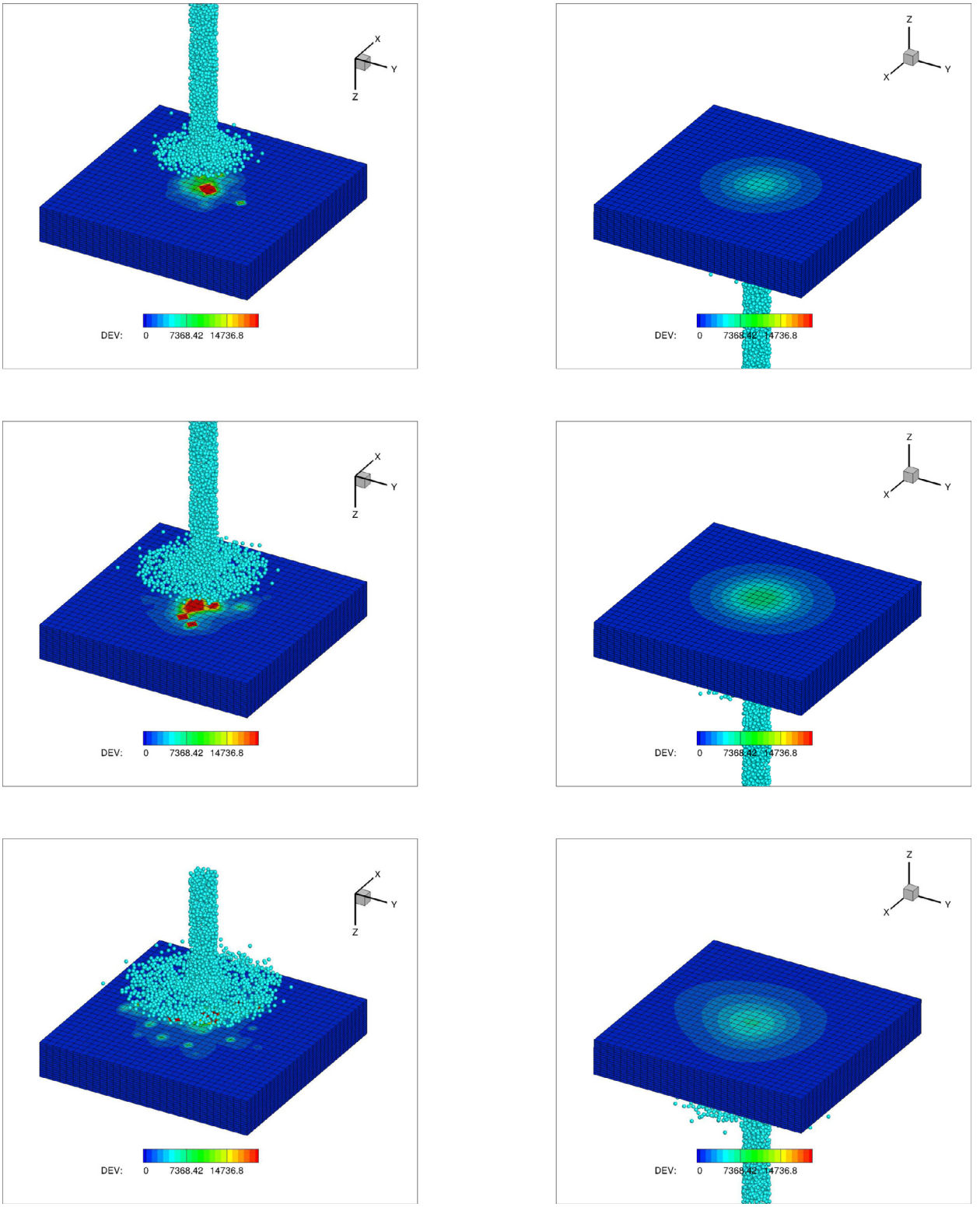

Fig. 7. Example: Deposition onto a surface. The substrate colors indicate the norm of the total summed deviatoric stresses. Both the top (left) and bottom (right) are shown. The localized nature of the surface stresses are smeared out with increasing depth.

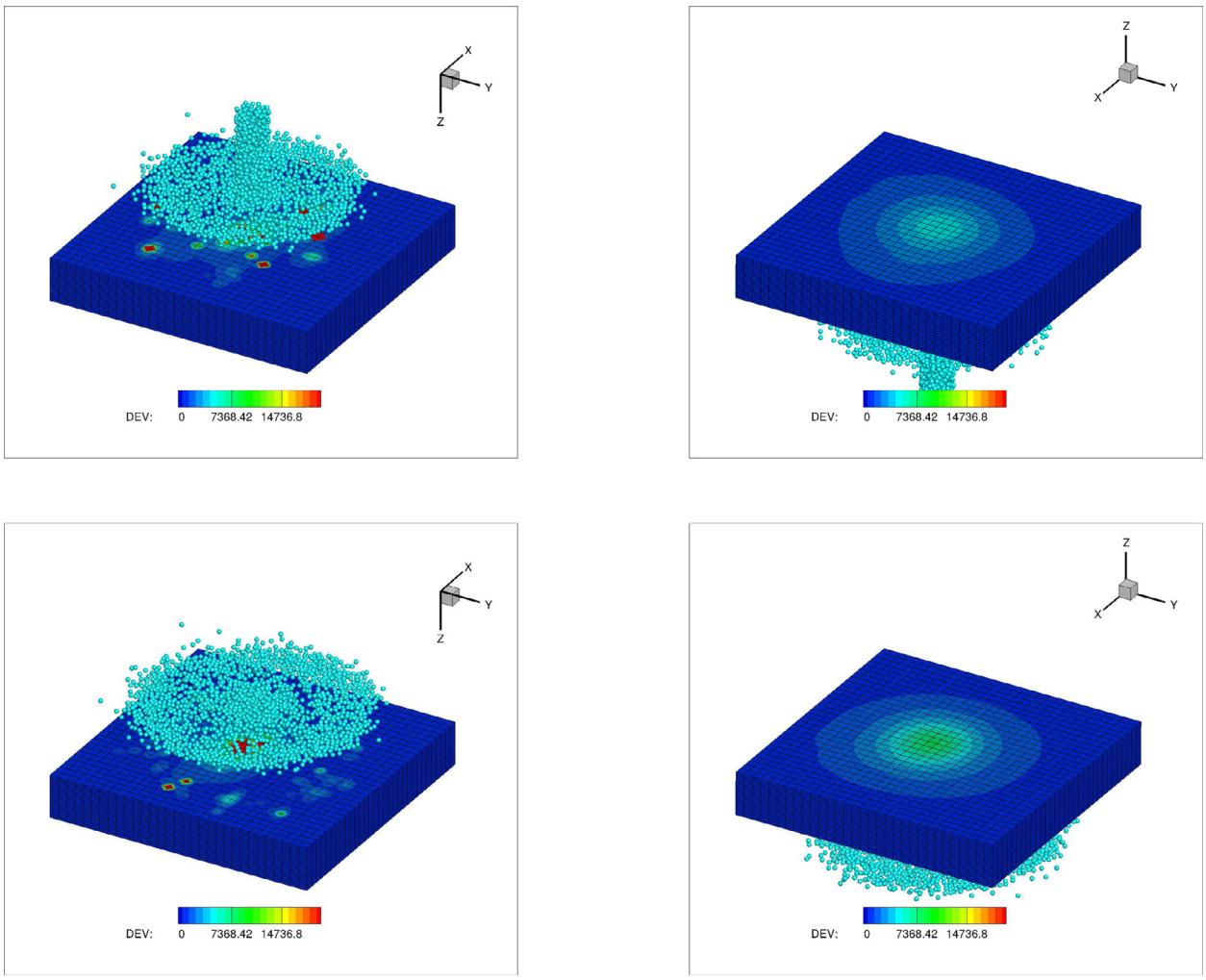

Fig. 8. Example: Deposition onto a surface. The substrate colors indicate the norm of the total summed deviatoric stresses. Both the top (left) and bottom (right) are shown. The localized nature of the surface stresses are smeared out with increasing depth.

a thorough analysis of this topic, including thermo-mechanical heat generation. We also remark that the present analysis can be used to investigate shot-peening processes. We refer the reader to Afazov, Becker, and Hyde (2012), Bagherifard, Giglio, Giudici, and Guagliano (2010), Elbella, Fadul, Uddanda, and Kasarla (2012) and Chen, Yang, and Meguid (2014) for the finite element analysis of the response of the substrate of a shot-peened solid and recently to Zohdi (2015b) for rapid computation of multiple contacting bodies on substrates for additive particle printing processes.

5. Summary, conclusions and extensions

In summary, this paper developed a computational-mechanics framework to investigate the deposition of streams of particles onto compliant substrates. Substrate stresses due to multiple surface particle contact events were efficiently computed by superposing individual particle contact solutions coupled to a multibody dynamics formulation for the interacting particles. In particular:

- A multibody collision model was developed to determine the interaction of the particles with each other, as well as with the substrate.
- Classical Boussinesq-like point-load solutions on a half-space were used to represent the contribution of each particle to the total stresses on the substrate.

The modeling approach allows for rapid computation of deposition-induced stresses which allows one to conduct parameter studies, leaving more intensive numerical methods, such as Finite Element methods, for more detailed studies, if needed. Three-dimensional examples were provided to illustrate the technique. The utility of the approach is that one can very rapidly compute the results of the action of a given set of process parameters and thus run several “forward” problems for optimization studies.

We remark that there are several manufacturing applications where particles are deposited onto substrates. However, there are variants which also utilize imprint lithography as a means of decreasing the feature size of patterned particles while allowing more precise control over the structure of the print (Ko et al., 2007, 2008; Park et al., 2007 and Park et al., 2008). In this fabrication method, the particle-laden inks are patterned by pressing with an elastomer mold and the particles are dried into their final configuration. While the resolution of imprint lithography is improved over inkjet printing, there exists a residual layer on the substrate that must be etched away after patterning. Control over the height of features can be corrupted by capillary action between the mold and the drying ink, in particular along the length of longer features. Thus, as a possible alternative to imprint lithography, particle self-assembly methods, based on capillary filling of photoresist templates have been proposed (Demko et al., 2012; Demko et al., 2010), and appear to be promising. It is important to realize that in many cases particles are charged (ionized) or magnetized and guided to a surface. In these cases, the particles may bond and stick to one-another and to the surface. Thus, as an extension, we consider the equation of motion for the i^{th} particle in system

$$m_i\ddot{\boldsymbol{r}}_i = \boldsymbol{\Psi}_i^{tot}(\boldsymbol{r}_1, \boldsymbol{r}_2, \ldots, \boldsymbol{r}_{N_p}) = \boldsymbol{\Psi}_i^{con} + \boldsymbol{\Psi}_i^{subs} + \boldsymbol{\Psi}_i^{bond} + \boldsymbol{\Psi}_i^{damp} + \boldsymbol{\Psi}_i^{e+m}, \tag{25}$$

where the last term represents electromagnetic contributions, such as (1) Lorentz forces (for charged particles), (2) magnetic forces (for magnetic particles) and (3) inter-particle near-field forces. The inclusion of the effects are described in detail in the Appendix C and under current investigation by the author.

Acknowledgments

This work was funded in part by the Army Research Laboratory through the Army High Performance Computing Research Center (cooperative agreement W911NF-07-2-0027).

Appendix A. Numerical solution of a multiparticle system

A1. Temporal discretization

Integrating Eq. (25) leads to (using a trapezoidal rule with variable integration metric, $0 \leq \phi \leq 1$)

$$\begin{aligned}\boldsymbol{v}_i(t+\Delta t) &= \boldsymbol{v}_i(t) + \frac{1}{m_i}\int_t^{t+\Delta t} \boldsymbol{\Psi}_i^{tot}\, dt \\ &\approx \boldsymbol{v}_i(t) + \frac{\Delta t}{m_i}\Big(\phi\boldsymbol{\Psi}_i^{tot}(t+\Delta t) + (1-\phi)\boldsymbol{\Psi}_i^{tot}(t)\Big),\end{aligned} \tag{26}$$

where $\boldsymbol{\Psi}_i^{tot} = \boldsymbol{\Psi}_i^{con} + \boldsymbol{\Psi}_i^{subs} + \boldsymbol{\Psi}_i^{bond} + \boldsymbol{\Psi}_i^{damp}$. The position can be computed via application of the trapezoidal rule again:

$$\boldsymbol{r}_i(t+\Delta t) \approx \boldsymbol{r}_i(t) + \Delta t(\phi\boldsymbol{v}_i(t+\Delta t) + (1-\phi)\boldsymbol{v}_i(t)), \tag{27}$$

which can be consolidated into

$$\boldsymbol{r}_i(t+\Delta t) = \boldsymbol{r}_i(t) + \boldsymbol{v}_i(t)\Delta t + \frac{\phi(\Delta t)^2}{m_i}(\phi\boldsymbol{\Psi}_i^{tot}(t+\Delta t) + (1-\phi)\boldsymbol{\Psi}_i^{tot}(t)). \tag{28}$$

This leads to a coupled system of equations, which are solved using an adaptive iterative scheme, building on approaches found in various forms in Zohdi (2014a, 2002, 2005, 2007, 2010, 2012, 2013a, 2013b, 2014b, 2014c, 2014d, 2015a, 2015b); Zohdi and Wriggers (2008). We note that the material contact compliance constants in the various force terms could be functions of temperature, $K = K(\Theta)$, where Θ is the temperature, although a fully coupled thermal model is not considered here. We refer the reader to Zohdi (2014b, 2014c) for more details.

A2. Iterative (implicit) solution method

Following the basic framework in Zohdi (2014a, 2002, 2005, 2007, 2010, 2012, 2013a, 2013b, 2014b, 2014c, 2014d, 2015a, 2015b); Zohdi and Wriggers (2008), we write Eq. (28) in a slightly more streamlined form for particle i

$$\boldsymbol{r}_i^{L+1} = \boldsymbol{r}_i^L + \boldsymbol{v}_i^L\Delta t + \frac{\phi(\Delta t)^2}{m_i}\Big(\phi(\boldsymbol{\Psi}_i^{tot,L+1}) + (1-\phi)(\boldsymbol{\Psi}^{tot,L})\Big), \tag{29}$$

which leads to a coupled set equations for $i = 1, 2 \ldots N_p$ particles, where the superscript L is a time interval counter. The set of equations represented by Eq. (29) can be solved recursively. Eq. (29) can be solved recursively by recasting the relation as

$$\boldsymbol{r}_i^{L+1,K} = \boldsymbol{r}_i^L + \boldsymbol{v}_i^L\Delta t + \frac{(\phi\Delta t)^2}{m_i}\boldsymbol{\Psi}_i^{tot,L+1,K-1} + \frac{\phi(\Delta t)^2}{m_i}(1-\phi)\boldsymbol{\Psi}_i^{tot,L}, \tag{30}$$

which is of the form

$$\boldsymbol{r}_i^{L+1,K} = \mathcal{G}(\boldsymbol{r}_i^{L+1,K-1}) + \mathcal{R}_i, \tag{31}$$

where $K = 1, 2, 3, \ldots$ is the index of iteration within time step $L+1$ and

- $\boldsymbol{\Psi}_i^{tot,L+1,K-1} \stackrel{\text{def}}{=} \boldsymbol{\Psi}_i^{tot,L+1,K-1}(\boldsymbol{r}_1^{L+1,K-1}, \boldsymbol{r}_2^{L+1,K-1} \dots \boldsymbol{r}_N^{L+1,K-1})$,
- $\boldsymbol{\Psi}_i^{tot,L} \stackrel{\text{def}}{=} \boldsymbol{\Psi}_i^{tot,L}(\boldsymbol{r}_1^{L}, \boldsymbol{r}_2^{L} \dots \boldsymbol{r}_N^{L})$,
- $\mathcal{G}(\boldsymbol{r}_i^{L+1,K-1}) = \frac{(\phi \Delta t)^2}{m_i} \boldsymbol{\Psi}_i^{tot,L+1,K-1}$ and
- $\mathcal{R}_i = \boldsymbol{r}_i^L + \boldsymbol{v}_i^L \Delta t + \frac{\phi(\Delta t)^2}{m_i}(1-\phi)\boldsymbol{\Psi}_i^{tot,L}$.

The term $\mathcal{R}_i$ is a remainder term that does not depend on the solution. The convergence of such a scheme is dependent on the behavior of $\mathcal{G}$. Namely, a sufficient condition for convergence is that $\mathcal{G}$ is a contraction mapping for all $\boldsymbol{r}_i^{L+1,K}$, $K = 1, 2, 3 \dots$. In order to investigate this further, we define the iteration error as

$$\boldsymbol{\varpi}_i^{L+1,K} \stackrel{\text{def}}{=} \boldsymbol{r}_i^{L+1,K} - \boldsymbol{r}_i^{L+1}. \tag{32}$$

A necessary restriction for convergence is iterative self consistency, i.e. the "exact" (discretized) solution must be represented by the scheme, $\boldsymbol{r}_i^{L+1} = \mathcal{G}(\boldsymbol{r}_i^{L+1}) + \mathcal{R}_i$. Enforcing this restriction, a sufficient condition for convergence is the existence of a contraction mapping

$$|| \underbrace{\boldsymbol{r}_i^{L+1,K} - \boldsymbol{r}_i^{L+1}}_{\boldsymbol{\varpi}_i^{L+1,K}} || = ||\mathcal{G}(\boldsymbol{r}_i^{L+1,K-1}) - \mathcal{G}(\boldsymbol{r}_i^{L+1})|| \leq \eta^{L+1,K} ||\boldsymbol{r}_i^{L+1,K-1} - \boldsymbol{r}_i^{L+1}||, \tag{33}$$

where, if $0 \leq \eta^{L+1,K} < 1$ for each iteration K, then $\boldsymbol{\varpi}_i^{L+1,K} \rightarrow \boldsymbol{0}$ for any arbitrary starting value $\boldsymbol{r}_i^{L+1,K=0}$, as $K \rightarrow \infty$, which is a contraction condition that is sufficient, but not necessary, for convergence. The convergence of Eq. (30) is scaled by $\eta \propto \frac{(\phi \Delta t)^2}{m_i}$. Therefore, we see that the contraction constant of $\mathcal{G}$ is:

- Directly dependent on the magnitude of the interaction forces ($||\boldsymbol{\Psi}||$).
- Inversely proportional to the masses m_i and
- Directly proportional to $(\Delta t)^2$.

Thus, decreasing the time step size improves the convergence. *In order to maximize the time-step sizes (to decrease overall computing time) and still meet an error tolerance on the numerical solution's accuracy*, we build on an approach originally developed for continuum thermo-chemical multifield problems (Zohdi, 2002), where one assumes: (1) $\eta^{L+1,K} \approx S(\Delta t)^p$, ($S$ is a constant) and (2) the error within an iteration behaves according to $(S(\Delta t)^p)^K \varpi^{L+1,0} = \varpi^{L+1,K}$, $K = 1, 2, \dots$, where $\varpi^{L+1,0} = \boldsymbol{r}^{L+1,K=1} - \boldsymbol{r}^L$ is the initial norm of the iterative (relative) error and S is intrinsic to the system. For example, for second-order problems, due to the quadratic dependency on Δt, $p \approx 2$. The objective is to meet an error tolerance in exactly a preset (the analyst sets this) number of iterations. To this end, one writes $(S(\Delta t_{\text{tol}})^p)^{K_d} \varpi^{L+1,0} = TOL$, where TOL is a tolerance and where K_d is the number of desired iterations. If the error tolerance is not met in the desired number of iterations, the contraction constant $\eta^{L+1,K}$ is too large. Accordingly, one can solve for a new smaller step size, under the assumption that S is constant,

$$\Delta t_{\text{tol}} = \Delta t \left(\frac{(\frac{TOL}{\varpi^{L+1,0}})^{\frac{1}{pK_d}}}{(\frac{\varpi^{L+1,K}}{\varpi^{L+1,0}})^{\frac{1}{pK}}} \right) \stackrel{\text{def}}{=} \Delta t \Lambda_K. \tag{34}$$

The assumption that S is constant is not critical, since the time steps are to be recursively refined and unrefined throughout the simulation. Clearly, the expression in Eq. (34) can also be used for time step enlargement, if convergence is met in less than K_d iterations (typically chosen to be between five to ten iterations).

A3. Algorithm

The solution steps are, within a time-step:

- (1): Start a global fixed iteration (set $i = 1$ (particle counter) and $K = 0$ (iteration counter))
- (2): If $i > N_p$ then go to (4)
- (3): If $i \leq N_p$ then:
  - (a) Compute the position $\boldsymbol{r}_i^{L+1,K}$
  - (b) Go to (2) for the next particle ($i = i + 1$)
- (4): Measure error (normalized) quantities
  - (a) $\varpi_K \stackrel{\text{def}}{=} \frac{\sum_{i=1}^{N_p} ||\boldsymbol{r}_i^{L+1,K} - \boldsymbol{r}_i^{L+1,K-1}||}{\sum_{i=1}^{N_p} ||\boldsymbol{r}_i^{L+1,K} - \boldsymbol{r}_i^{L}||}$
  - (b) $Z_K \stackrel{\text{def}}{=} \frac{\varpi_K}{TOL_r}$
  - (c) $\Lambda_K \stackrel{\text{def}}{=} \left(\frac{(\frac{TOL}{\varpi_0})^{\frac{1}{pK_d}}}{(\frac{\varpi_K}{\varpi_0})^{\frac{1}{pK}}} \right)$
- (5): If the tolerance is met: $Z_K \leq 1$ and $K < K_d$ then

(a) Increment time: $t = t + \Delta t$
(b) Construct the next time step: $(\Delta t)^{new} = \Lambda_K (\Delta t)^{old}$,
(c) Select the minimum size: $\Delta t = \textbf{MIN}((\Delta t)^{lim}, (\Delta t)^{new})$ and go to (1)

- (6): If the tolerance is not met: $Z_K > 1$ and $K < K_d$ then
  (a) Update the iteration counter: $K = K + 1$
  (b) Reset the particle counter: $i = 1$
  (c) (c) Go to (2)
- (7): If the tolerance is not met ($Z_K > 1$) and $K = K_d$ then
  (a) Construct a new time step: $(\Delta t)^{new} = \Lambda_K (\Delta t)^{old}$
  (b) Restart at time t and go to (1)

Time-step size adaptivity is critical, since the system's dynamics and configuration can dramatically change over the course of time, possibly requiring quite different time step sizes to control the iterative error. However, to maintain the accuracy of the time-stepping scheme, one must respect an upper bound dictated by the discretization error, i.e., $\Delta t \leq \Delta t^{lim}$. Note that in step (5), Λ_K may enlarge the time-step if the error is lower than the preset tolerance.

Remark. Although thermal effects were not considered, the algorithm can be modified to account for coupled thermal effects. In those cases, the parameters, such as K_{pij} can be thermally dependent since the particles can thermally soften. For example, the compliance constant for the particles in the contact law can be written as (here Θ is the temperature):

$$K_{pi} = \textbf{MAX}\left(K_{pio}\left(e^{-a_i(\frac{\Theta_i}{\Theta_i^*}-1)} \right), K_{pi}^{lim} \right), \tag{35}$$

and for particle j

$$K_{pj} = \textbf{MAX}\left(K_{pjo}\left(e^{-a_j(\frac{\Theta_j}{\Theta_j^*}-1)} \right), K_{pj}^{lim} \right), \tag{36}$$

and take the average at the interface and the value in the contact law:

$$K_{pij} = \frac{1}{2}\left(K_{pi} + K_{pj} \right). \tag{37}$$

There is a multitude of possible representations, and it is relatively easy to select one or the other, and to embed in the staggering framework developed. A fully coupled thermal model is not considered here, and we refer the reader to Zohdi (2014b) for more details.

Appendix B. contact area parameter and alternative models

B1. Contact area parameter

Following (Zohdi, 2014b, 2014c), and referring to Fig. B.9, one can solve for an approximation of the common contact radius a_{ij} (and the contact area, $A_{ij}^c = \pi a_{ij}^2$) by solving the following three equations,

$$a_{ij}^2 + L_i^2 = R_i^2, \tag{38}$$

and

$$a_{ij}^2 + L_j^2 = R_j^2, \tag{39}$$

and

$$L_i + L_j = ||\boldsymbol{r}_i - \boldsymbol{r}_j||, \tag{40}$$

where R_i is the radius of particle i, R_j is the radius of particle j, L_i is the distance from the center of particle i and the common contact interpenetration line and L_j is the distance from the center of particle j and the common contact interpenetration line, where the extent of interpenetration is

$$\delta_{ij} = R_i + R_j - ||\boldsymbol{r}_i - \boldsymbol{r}_j||. \tag{41}$$

The above equations yield an expression a_{ij}, which yields an expression for the contact area parameter

$$A_{ij}^c = \pi a_{ij}^2 = \pi (R_i^2 - L_i^2), \tag{42}$$

where

$$L_i = \frac{1}{2}\left(||\boldsymbol{r}_i - \boldsymbol{r}_j|| - \frac{R_j^2 - R_i^2}{||\boldsymbol{r}_i - \boldsymbol{r}_j||} \right). \tag{43}$$

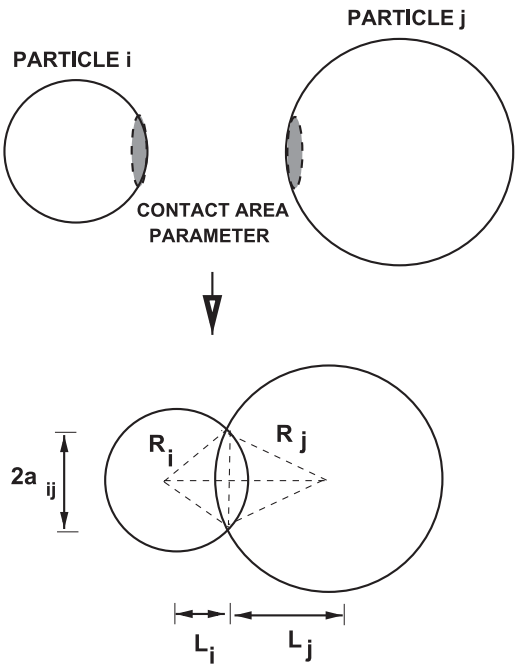

Fig. B9. An approximation of the contact area parameter for two particles in contact (Zohdi, 2014b, 2014c).

B2. Aternative models

One could easily construct more elaborate relations connecting the relative proximity of the particles and other metrics to the contact force, $\boldsymbol{\Psi}_{ij}^{con,n} \propto \mathcal{F}(\boldsymbol{r}_i, \boldsymbol{r}_j, \boldsymbol{n}_{ij}, R_i, R_j, \dots)$, building on, for example, Hertzian contact models. This poses no difficulty in the direct numerical method developed. For the remainder of the analysis, we shall use the deformation metric in Eq. 8. For detailed treatments, see Wellmann, Lillie, and Wriggers (2008a, 2008b, 2008c); Wellmann and Wriggers (2012); Wellmann, Wriggers, Onate, and Owen (2011) and (Avci & Wriggers, 2012). We note that with the appropriate definition of parameters, one can recover Hertz, Bradley, Johnson–Kendel–Roberts, Derjaguin–Muller–Toporov contact models. For example, Hertzian contact is widely used, with the assumptions being

- Frictionless, continuous, surfaces.
- Each of contacting bodies are elastic half-spaces, whereby the contact area dimensions are smaller radii of the bodies and.
- The bodies remain elastic (infinitesimal strains).

results in the following contact force:

$$\boldsymbol{\Psi}_{ij}^{con,n} = \frac{4}{3}(R^*)^{1/2} E^* \delta_{ij}^{3/2}, \tag{44}$$

which has the general form of $\boldsymbol{\Psi}^{con,n} = K_{ij}^* \delta_{ij}^p$, where

- $R^* = \left(\frac{1}{R_i} + \frac{1}{R_j}\right)^{-1}$ and
- $E^* = \left(\frac{1-\nu_i^2}{E_i} + \frac{1-\nu_j^2}{E_j}\right)^{-1}$,

where E is the Young's modulus and ν is the Poisson ratio, The contact area with such a model has already been incorporated in the relation above, and is equal to $A_{ij}^c = \pi a^2$ where $a = \sqrt{R^* \delta_{ij}}$. For more details, we refer the reader to Johnson (1985). Furthermore, we remark that the normal contact between a particle and a substrate, with a Hertzian model is given by

$$\boldsymbol{\Psi}_{i}^{subs,n} = \frac{4}{3}(R^*)^{1/2} E^* \delta_{iw}^{3/2} = K_{iw}^* \delta_{iw}^p, \tag{45}$$

where $R_j = R_w = \infty$ (see Eq. (44))

- $R^* = R_i$ and
- $E^* = \left(\frac{1-\nu_i^2}{E_i} + \frac{1-\nu_j^2}{E_j}\right)^{-1}$.

It is obvious that for a deeper understanding of the deformation within a particle, it must be treated as a deformable continuum, which would require a highly-resolved spatial discretization, for example using the Finite Element Method for the contacting bodies. This requires a large computational effort. For the state of the art in Finite Element Methods and Contact Mechanics, see the books of Wriggers (2002, 2008). For work specifically focusing on the continuum mechanics of particles, see Zohdi and Wriggers (2008).

Appendix C. Nonstandard effects-particle ionization and magnetization

Following (Zohdi, 2012), electromagnetic forces can be decomposed into three contributions, (1) Lorentz forces (for charged particles), (2) magnetic forces (for magnetic particles) and (3) inter-particle near-field forces. We will utilize the decomposition of the electromagnetic forces generated into a (inter-particle) near-field interaction and the external electromagnetic field

$$\boldsymbol{\Psi}_i^{e+m} = \boldsymbol{\Psi}_i^{lor,e+m} + \boldsymbol{\Psi}_i^{mag} + \underbrace{\sum_{j\neq i}^{N} \boldsymbol{\psi}_{ij}^{nf}}_{\boldsymbol{\Psi}_i^{nf}} + = \underbrace{q_i(\boldsymbol{E}^{ext} + \boldsymbol{v}_i \times \boldsymbol{B}^{ext})}_{\boldsymbol{\Psi}_i^{lor,e+m}} + \boldsymbol{\Psi}_i^{mag} + \boldsymbol{\Psi}_i^{nf}, \tag{46}$$

where $\sum_{j\neq i}^{N} \boldsymbol{\psi}_{ij}^{nf}$ represents the interaction between particle i and all other particles $j = 1,\ 2 \ldots N\ (j \neq i)$, $\boldsymbol{\Psi}_i^{lor,e+m}$ represents external Lorentz-induced forces from the surrounding environment, for example comprised of $\mathbf{E}^{ext}$ and $\mathbf{B}^{ext}$, which are externally-controlled fields that are independent of the response of the system. The terms $\mathbf{E}^{ext}$ and $\mathbf{B}^{ext}$ can be considered as static (or extremely slowly-varying), and thus mutually uncoupled and independently controllable. The self-induced magnetic fields developed between particles is insignificant for the velocity ranges of interest here (well below the speed of light). For the Lorentz force, we recall the following important observations in conjunction with electromagnetic phenomena (Jackson, 1998):

- If a point charge q experiences a force $\boldsymbol{\Psi}^{lor,\,e}$, the electric field, $\mathbf{E}^{ext}$, at the location of the charge is defined by $\boldsymbol{\Psi}^{lor,e} = q\boldsymbol{E}^{ext}$.
- If the charge is moving, another force may arise, $\boldsymbol{\Psi}^{lor,\,m}$, which is proportional to its velocity $\mathbf{v}$. This other (induced) field is denoted as the "magnetic induction" or just the "magnetic field", $\mathbf{B}^{ext}$, such that $\boldsymbol{\Psi}^{lor,m} = q\boldsymbol{v} \times \boldsymbol{B}^{ext}$.
- If the forces occur concurrently (the charge is moving through the region possessing both electric and magnetic fields), then the electromagnetic force is $\boldsymbol{\Psi}^{lor,e+m} = q\boldsymbol{E}^{ext} + q\boldsymbol{v} \times \boldsymbol{B}^{ext}$.

C1. Inter-particle near-field interaction

Following (Zohdi, 2012), a simple form that captures the essential near-field effects is

$$\boldsymbol{\Psi}_i^{nf} = \sum_{j\neq i}^{N_p} \left(\underbrace{\alpha_{1ij} ||\boldsymbol{r}_i - \boldsymbol{r}_j||^{-\beta_1}}_{\text{attraction}} - \underbrace{\alpha_{2ij} ||\boldsymbol{r}_i - \boldsymbol{r}_j||^{-\beta_2}}_{\text{repulsion}} \right) \boldsymbol{n}_{ij}, \tag{47}$$

where the α's and β's are empirical material parameters. The various representations (decompositions) of the coefficients that appear in Eq. (47) are with $c_i = \pm 1$ (a positive/negative identifier)

- mass-based (m = mass): $\alpha_{ij} = \bar{\alpha}_{ij} m_i m_j c_i c_j$,
- surface area-based (a = surface area): $\alpha_{ij} = \bar{\alpha}_{ij} a_i a_j c_i c_j$,
- volume-based (V = volume): $\alpha_{ij} = \bar{\alpha}_{ij} V_i V_j c_i c_j$ and
- charge-based: $\alpha_{ij} = \bar{\alpha}_{ij} q_i q_j c_i c_j$,

where the $\bar{\alpha}_{ij}$ are empirical material parameters. There are vast numbers of empirical representations, for example, found in the field of "Molecular Dynamics" (MD), which typically refers to mathematical models of systems of atoms or molecules where each atom (or molecule) is represented by a material point and is treated as a point mass. The overall motion of such mass-point systems is dictated by Newtonian mechanics. For an extensive survey of MD-type interaction forces, which includes comparisons of the theoretical and computational properties of a variety of interaction laws, we refer the reader to Frenklach and Carmer (1999). In the usual MD approach (see Haile, 1992, for example), the motion of individual atoms is described by Newton's second law with the forces computed from differentiating a prescribed potential energy function, with applications to solids, liquids, and gases, as well as biological systems (Hase, 1999; Schlick, 2000) and (Rapaport, 1995). The interaction functions usually take the form of the familiar Mie, Lennard-Jones, and Morse potentials (Moelwyn-Hughes, 1961), however three-body terms can be introduced directly into the interaction functions (Stillinger & Weber, 1985) or, alternatively, "local" modifications can be made to two-body representations (Tersoff, 1988).

C2. Magnetic forces

An additional force can be exerted on magnetic particles, independent of the electrodynamically-induced Lorentz forces. A relatively simple model for the charcterization of this force is given by

$$\boldsymbol{\Psi}^{mag} = \nabla(\gamma \boldsymbol{B}^{ext} \cdot \boldsymbol{B}^{ext}), \tag{48}$$

where γ is a material parameter that is related to the magnetization of the particle, and which is dependent on the magnetic dipole properties, the magnetic susceptibility, the magnetic permeability and the internal magnetic moment density of the material (see Boyer, 1988; Cullity, 2008; Feynman, Leighton, and Sands, 2006 or Jackson, 1998. For the specific applications in this paper, Ψ_i^{mag} is considered small. The inclusion of the effects outlined in this summary are under investigation by the author.

References

Abedian, B., & Kachanov, M. (2010). *On the effective viscosity of suspensions International Journal of Engineering Science, 48*(11), 962–965. doi:10.1016/j.ijengsci.2010.08.012.

Afazov, S. M., Becker, A. A., & Hyde, T. H. (2012). Mathematical modeling and implementation of residual stress mapping from microscale to macroscale finite element models. *The Journal of Manufacturing Science and Engineering, 134*(2). 021001-021001-11.

Ahmad, Z., Rasekh, M., & Edirisinghe, M. (2010). Electrohydrodynamic direct writing of biomedical polymers and composites. *Macromolecular Materials and Engineering, 295*, 315–319.

Avci, B., & Wriggers, P. (2012). A dem-fem coupling approach for the direct numerical simulation of 3d particulate flows. *Journal of Applied Mechanics, 79*(010901), 1–7.

Bagherifard, S., Giglio, M., Giudici, L., & Guagliano, M. (2010). Experimental and numerical analysis of fatigue properties improvement in a titanium alloy by shot peening proc. asme. 49163. *ASME 2010 10th Biennial Conference on Engineering Systems Design and Analysis, 2*, 317–322.

Bolintineanu, D. S., Grest, G. S., Lechman, J. B., Pierce, F., Plimpton, S. J., & Schunk, P. R. (2014). Particle dynamics modeling methods for colloid suspensions. *Computational Particle Mechanics, 1*(3), 321–356.

Boussinesq, J. (1885). *Application des Potentials a l' etude de l' equilibre et du mouvement des solides elastiques: Vol. 45* p. 108. Paris: Gauthier-Villars.

Boyer, T. H. (1988). The force on a magnetic dipole. *American Journal of Physics, 56*(8), 688–692. doi:10.1119/1.15501. Bibcode:1988AmJPh..56..688B

Cante, J., Davalos, C., Hernandez, J. A., Oliver, J., Jonsen, P., Gustafsson, G., & Haggblad, H. A. (2014). Pfem-based modeling of industrial granular flows. *Computational Particle Mechanics, 1*(1), 47–70.

Carbonell, J. M., Onate, E., & Suarez, B. (2010). Modeling of ground excavation with the particle finite element method. *Journal of Engineering Mechanics, ASCE, 136*, 455–463.

Chen, Z., Yang, F., & Meguid, S. A. (2014). Realistic finite element simulations of arc-height development in shot-peened almen strips j. *Engineering Materials and Technology, 136*(4). 041002–041002

Choi, S., Jamshidi, A., Seok, T. J., Zohdi, T. I., Wu. , M. C., & Pisano, A. P. (2012). Fast, high-throughput creation of size-tunable micro, nanoparticle clusters via evaporative self-assembly in picoliter-scale droplets of particle suspension. *Langmuir, 28*(6), 3102–3111.

Choi, S., Park, I., Hao, Z., Holman, H. Y., Pisano, A. P., & Zohdi, T. I. (2010a). Ultra-fast self-assembly of micro-scale particles by open channel flow. *Langmuir, 26*(7), 4661–4667.

Choi, S., Pisano, A. P., & I. , Z. T. (2013). An analysis of evaporative self-assembly of micro particles in printed picoliter suspension droplets. *Journal of Thin Solid Films, 537*(30), 180–189.

Choi, S., Stassi, S., Pisano, A. P., & Zohdi, T. I. (2010b). Coffee-ring effect-based three dimensional patterning of micro, nanoparticle assembly with a single droplet. *Langmuir, 26*(14), 11690–11698.

Cullity, C. D. G. (2008). *Introduction to magnetic materials* (2nd ed., p. 103). Wiley-IEEE Press. ISBN 0-471-47741-9.

Demko, M., Choi, S., Zohdi, T. I., & Pisano, A. P. (2012). High resolution patterning of nanoparticles by evaporative self-assembly enabled by in-situ creation and mechanical lift-off of a polymer template. *Applied Physics Letters, 99*. 253102-1-253102-3

Demko, M. T., Cheng, J. C., & Pisano, A. P. (2010). High-resolution direct patterning of gold nanoparticles by the microfluidic molding process. *Langmuir*, 412–417.

Donev, A., Cisse, I., Sachs, D., Variano, E. A., Stillinger, F., Connelly, R., … Chaikin, P. (2004a). Improving the density of jammed disordered packings using ellipsoids. *Science, 13*, 990–993. February 2004, Vol. 303

Donev, A., Stillinger, F. H., Chaikin, P. M., & Torquato, S. (2004b). Unusually dense crystal ellipsoid packings. *Physical Review Letters, 92*, 255506.

Donev, A., Torquato, S., & Stillinger, F. (2005). Neighbor list collision-driven molecular dynamics simulation for nonspherical hard particles-i. algorithmic details. *Journal of Computational Physics, 202*, 737.

Dwivedi, G., Wentz, T., Sampath, S., & Nakamura, T. (2010). Assessing process and coating reliability through monitoring of process and design relevant coating properties. *J. Thermal Spray Technology, 19*, 695–712.

Elbella, A., Fadul, F., Uddanda, S. H., & Kasarla, N. R. (2012). Influence of shot peening parameters on process effectiveness. In *Proc. asme. 45196; volume 3: Design, materials and manufacturing, parts a, b, and c:2015-2021*.

Fathi, S., Dickens, P., Khodabakhshi, K., & Gilbert, M. (2013). Microcrystal particles behaviour in inkjet printing of reactive nylon materials j. *Manuf. Sci. Eng., 135*, 011009. doi:10.1115/1.4023272.

Feynman, R. P., Leighton, R. B. Sands, M. (2006). The Feynman Lectures on Physics 2. ISBN 0-8053-9045-6.

Frenklach, M., & Carmer, C. S. (1999). Molecular dynamics using combined quantum & empirical forces: application to surface reactions. *Advances in classical trajectory methods, 4*, 27–63.

Fuller, S. B., Wilhelm, E. J., & Jacobson, J. M. (2002). Ink-jet printed nanoparticle microelectromechanical systems. *Journal of Microelectromechanical Systems, 11*, 54–60.

Gamota, D., Brazis, P., Kalyanasundaram, K., & Zhang, J. (2004). *Printed Organic and Molecular Electronics*. New York: Kluwer Academic Publishers.

Grekov, M. A., & Kostyrko, S. A. (2015). A multilayer film coating with slightly curved boundary. *International Journal of Engineering Science, 89*, 61–74.

Haile, J. M. (1992). *Molecular Dynamics Simulations: Elementary Methods*. Wiley.

Hase, W. L. (1999). Molecular Dynamics of Clusters, Surfaces, Liquids, & Interfaces. *Advances in classical trajectory methods*: Volume 4. JAI Press.

Huang, D., Liao, F., Molesa, S., Redinger, D., & Subramanian, V. (2003). Plastic-compatible low-resistance printable gold nanoparticle conductors for flexible electronics. *Journal of the Electrochemical Society, 150*(7), G412–417.

Huang, Y., Leu, M. C., Mazumdar, J., & Donmez, A. (2015). Additive manufacturing: current state, future potential, gaps and needs, and recommendation. *Journal of Manufacturing Science and Engineering, 137*. 014001-1

Jackson, J. D. (1998). *Classical Electrodynamics* (Third edition). Wiley.

Johnson, K. (1985). *Contact mechanics*. Cambridge University Press.

Kachanov, M., & Abedian, B. (2015). *On the isotropic viscosity of suspensions containing particles of diverse shapes and orientations, 94*, 71–85.

Kachanov, M., Shafiro, B., & Tsukrov, I. (2003). *Handbook of elasticity solutions*. Kluwer.

Kansaal, A., Torquato, S., & Stillinger, F. (2002). Diversity of order and densities in jammed hard-particle packings. *Physical Review E., 66*, 041109.

Ko, S. H., Park, I., Pan, H., Grigoropoulos, C. P., Pisano, A. P., Luscombe, C. K., et al. (2007). Direct nanoimprinting of metal nanoparticles for nanoscale electronics fabrication. *Nano Letters, 7*, 1869–1877.

Ko, S. H., Park, I., Pan, H., Misra, N., Rogers, M. S., Grigoropoulos, C. P., & Pisano, A. P. (2008). Zno nanowire network transistor fabrication by low temperature, all inorganic nanoparticle solution process. *Applied Physics Letters, 92*, 154102.

Labra, C., & Onate, E. (2009). High-density sphere packing for discrete element method simulations. *Communications in Numerical Methods in Engineering, 25*(7), 837–849.

Leonardi, A., Wittel, F. K., Mendoza, M., & Herrmann, H. J. (2014). Coupled dem-lbm method for the free-surface simulation of heterogeneous suspensions. *Computational Particle Mechanics, 1*(1), 3–13.

Liu, Y., Nakamura, T., Dwivedi, G., Valarezo, A., & Sampath, S. (2008). Anelastic behavior of plasma sprayed zirconia coatings. *Journal of American Ceramic Society, 91*, 4036–4043.

Liu, Y., Nakamura, T., Srinivasan, V., Vaidya, A., Gouldstone, A., & Sampath, S. (2007). Nonlinear elastic properties of plasma sprayed zirconia coatings and associated relationships to processing conditions. *Acta materialia, 55*, 4667–4678.
Martin, P. (2009). *Handbook of deposition technologies for films and coatings* (3rd ed.). Elsevier.
Martin, P. (2011). Introduction to surface engineering and functionally engineered materials. scrivener and elsevier. *Journal of Vacuum Science and Technology, A2*(2), 500.
Moelwyn-Hughes, E. A. (1961). *Physical Chemistry*. Pergamon.
Nakamura, T., & Liu, Y. (2007). Determination of nonlinear properties of thermal sprayed ceramic coatings via inverse analysis. *International Journal of Solids and Structures, 44*, 1990–2009.
Nakamura, T., Qian, G., & Berndt, C. C. (2000). Effects of pores on mechanical properties of plasma sprayed ceramic coatings. *Journal of American Ceramic Society, 83*, 578–584.
Nakanishi, H., Bishop, K. J. M., Kowalczyk, B., Nitzan, A., Weiss, E. A., Tretiakov, K. V., … Grzybowski, B. A. (2009). Photoconductance and inverse photoconductance in thin films of functionalized metal nanoparticles. *Nature, 460*, 371–375. 2009
Onate, E., Celigueta, M. A., Idelsohn, S. R., Salazar, F., & Suárez, B. (2011). Possibilities of the particle finite element method for fluid-soil-structure interaction problems. *Computational Mechanics, 48*, 307–318.
Onate, E., Celigueta, M. A., Latorre, S., Casas, G., Rossi, R., & Rojek, J. (2014). Lagrangian analysis of multiscale particulate flows with the particle finite element method. *Computational Particle Mechanics, 1*(1), 85–102.
Onate, E., Idelsohn, S. R., Celigueta, M. A., & Rossi, R. (2008). Advances in the particle finite element method for the analysis of fluid-multibody interaction and bed erosion in free surface flows. *Computer Methods in Applied Mechanics and Engineering, 197*(19-20), 1777–1800.
Park, I., Ko, S. H., Pan, H., Grigoropoulos, C. P., Pisano, A. P., Frechet, J. M. J., … Jeong, J. H. (2008). Nanoscale patterning and electronics on flexible substrate by direct nanoimprinting of metallic nanoparticles. *Advanced Materials, 20*, 489.
Park, J.-U., Hardy, M., Kang, S. J., Barton, K., Adair, K., Mukhopadhyay, D. K., … Rogers, J. A. (2007). High-resolution electrohydrodynamic jet printing. *Nature Materials, 6*, 782–789.
Qian, G., Nakamura, T., & Berndt, C. C. (1998). Effects of thermal gradient and residual stresses on thermal barrier coating fracture. *Mechanics of Materials, 27*, 91–110.
Rapaport, D. C. (1995). *The Art of Molecular Dynamics Simulation*. Cambridge University Press.
Rojek, J. (2014). Discrete element thermomechanical modelling of rock cutting with valuation of tool wear. *Computational Particle Mechanics, 1*(1), 71–84.
Rojek, J., Labra, C., Su, O., & Onate, E. (2012). Comparative study of different discrete element models and evaluation of equivalent micromechanical parameters. *International Journal of Solids and Structures, 49*, 1497–1517. doi:10.1016/j.ijsolstr.2012.02.032. 2012
Samarasinghe, S. R., Pastoriza-Santos, I., Edirisinghe, M. J., Reece, M. J., & Liz-Marzan, L. M. (2006). Printing gold nanoparticles with an electrohydrodynamic direct write device. *Gold Bulletin, 39*, 48–53.
Schlick, T. (2000). *Molecular modeling & simulation. An interdisciplinary guide*. New York: Springer-Verlag.
Sevostianov, I., & Kachanov, M. (2000). Modeling of the anisotropic elastic properties of plasma-sprayed coatings in relation to their microstructure. *Acta Materialia, 48*(6), 1361–1370.
Sevostianov, I., & Kachanov, M. (2001a). Plasma-sprayed ceramic coatings: Anisotropic elastic and conductive properties in relation to the microstructure. *Cross-Property Correlations. Materials Science and Engineering-A, 297*, 235–243.
Sevostianov, I., & Kachanov, M. (2001b). Thermal conductivity of plasma sprayed coatings in relation to their microstructure. *Journal of Thermal Spray Technology, 9*(4), 478–482.
Sevostianov, I., & Kachanov, M. (2012). Effective properties of heterogeneous materials: Proper application of the non-interaction and the "dilute limit" approximations. *The International Journal of Engineering Science, 58*, 124–128.
Sirringhaus, H., Kawase, T., Friend, R. H., Shimoda, T., Inbasekaran, M., Wu, W., & Woo, E. P. (2000). High-resolution inkjet printing of all-polymer transistor circuits. *Science, 290*, 2123–2126.
Stillinger, F. H., & Weber, T. A. (1985). Computer simulation of local order in condensed phases of silicon. *Phys. Rev. B, 31*, 5262–5271.
Tersoff, J. (1988). Empirical interatomic potential for carbon, with applications to amorphous carbon. *Phys. Rev. Lett., 61*, 2879–2882.
Torquato, S. (2002). *Random Heterogeneous Materials: Microstructure & Macroscopic Properties*. New York: Springer-Verlag.
Wang, J. Z., Zheng, Z. H., Li, H. W., Huck, W. T. S., & Sirringhaus, H. (2004). Dewetting of conducting polymer inkjet droplets on patterned surfaces. *Nature Materials, 3*, 171–176.
Wellmann, C., Lillie, C., & Wriggers, P. (2008a). Comparison of the macroscopic behavior of granular materials modeled by different constitutive equations on the microscale. *Finite Elements in Analysis and Design, 44*, 259–271.
Wellmann, C., Lillie, C., & Wriggers, P. (2008b). A contact detection algorithm for superellipsoids based on the common-normal concept. *Engineering Computations, 25*, 432–442.
Wellmann, C., Lillie, C., & Wriggers, P. (2008c). Homogenization of granular material modelled by a three-dimensional discrete element method. *Computers and Geotechnics, 35*, 394–405.
Wellmann, C., & Wriggers, P. (2012). A two-scale model of granular materials. *Computer Methods in Applied Mechanics and Engineering*, (46-58), 205–208.
Wellmann, C., & Wriggers, P. (2011). Homogenization of granular material modeled by a 3d dem. In E. Onate, & D. R. J. Owen (Eds.), *Particle-based methods: Fundamentals and applications* (pp. 211–231).
Widom, B. (1966). Random sequential addition of hard spheres to a volume. *Journal of Chemical Physics, 44*, 3888–3894.
Wriggers, P. (2002). *Computational contact mechanics*. John-Wiley.
Wriggers, P. (2008). *Nonlinear Finite Element Analysis*. Springer.
Zohdi, T. (2014a). Embedded electromagnetically sensitive particle motion in functionalized fluids. *Computational Particle Mechanics, 1*(1), 27–45.
Zohdi, T. I. (2002). An adaptive-recursive staggering strategy for simulating multifield coupled processes in microheterogeneous solids. *The International Journal of Numerical Methods in Engineering, 53*, 1511–1532.
Zohdi, T. I. (2005). Charge-induced clustering in multifield particulate flow. *The International Journal of Numerical Methods in Engineering, 62*(7), 870–898.
Zohdi, T. I. (2007). Computation of strongly coupled multifield interaction in particle-fluid systems. *Computer Methods in Applied Mechanics and Engineering, 196*, 3927–3950.
Zohdi, T. I. (2010). On the dynamics of charged electromagnetic particulate jets. *Archives of Computational Methods in Engineering, 17*(2), 109–135.
Zohdi, T. I. (2012). Dynamics of charged particulate systems. *Modeling, theory and computation*. Springer-Verlag.
Zohdi, T. I. (2013a). Numerical simulation of charged particulate cluster-droplet impact on electrified surfaces. *Journal of Computational Physics, 233*, 509–526.
Zohdi, T. I. (2013b). Rapid simulation of laser processing of discrete particulate materials. *Archives of Computational Methods in Engineering*, 1–17. doi:10.1007/s11831-013-9092-6.
Zohdi, T. I. (2014b). Additive particle deposition and selective laser processing-a computational manufacturing framework. *Computational Mechanics, 54*, 171–191.
Zohdi, T. I. (2014c). A direct particle-based computational framework for electrically-enhanced thermo-mechanical sintering of powdered materials. *Mathematics and Mechanics of Solids*, 1–21. doi:10.1007/s11831-013-9092-6.
Zohdi, T. I. (2014d). Rapid computation of statistically-stable particle/feature ratios for consistent substrate stresses in printed flexible electronics. *Journal of Manufacturing Science and Engineering, ASME* MANU-14-1476. doi:10.1115/1.4029327.
Zohdi, T. I. (2015a). Modeling and simulation of cooling-induced residual stresses in heated particulate mixture depositions. *Computational Mechanics*. doi:10.1007/s00466-015-1191-9.
Zohdi, T. I. (2015b). Modeling and simulation of the post-impact trajectories of particles in oblique precision shot-peening. *Computational Particle Mechanics*. doi:10.1007/s40571-015-0048-5.
Zohdi, T. I., & Wriggers, P. (2008). Introduction to computational micromechanics. *Second Reprinting*. Springer-Verlag.